Macromolecular Rapid Communications
www.mrc-journal.de

Enhancing the Biomimetic Mechanics of Bottlebrush Graft-Copolymers through Selective Solvent Annealing

*Akmal Z. Umarov, Joseph Collins, Evgeniia A. Nikitina, Ioannis Moutsios, Martin Rosenthal, Andrey V. Dobrynin, Sergei S. Sheiko, and Dimitri A. Ivanov**

Self-assembled networks of bottlebrush copolymers are promising materials for biomedical applications due to a unique combination of ultra-softness and strain-adaptive stiffening, characteristic of soft biological tissues. Transitioning from ABA linear-brush-linear triblock copolymers to A-g-B bottlebrush graft copolymer architectures allows significant increasing the mechanical strength of thermoplastic elastomers. Using real-time synchrotron small-angle X-ray scattering, it is shown that annealing of A-g-B elastomers in a selective solvent for the linear A blocks allows for substantial network reconfiguration, resulting in an increase of both the A domain size and the distance between the domains. The corresponding increases in the aggregation number and extension of bottlebrush strands lead to a significant increase of the strain-stiffening parameter up to 0.7, approaching values characteristic of the brain and skin tissues. Network reconfiguration without disassembly is an efficient approach to adjusting the mechanical performance of tissue-mimetic materials to meet the needs of diverse biomedical applications.

1. Introduction

Bottlebrush-based copolymers have attracted increasing interest due to their unique mechanical properties, combining ultra-softness with intense strain stiffening, which is characteristic of soft biological tissues.[1–6] For example, the skin feels soft on touch yet rapidly stiffens with deformation, generating the so-called J-shaped stress-strain curves, where the elastic modulus increases by up to 2–3 orders of magnitude.[7] Combining softness, firmness, strength, and damping in one material represents a difficult challenge for conventional linear-chain polymers due to the presence of chain entanglements and weak strain-stiffening.[8]

In contrast to linear chains, bottlebrush macromolecules demonstrate much lower entanglement densities,[9,10] providing access to very low mechanical moduli and a tunable strain-stiffening parameter,[11–13] which depends on side-chain length and grafting density. This makes bottlebrush-based copolymers promising candidates for applications in organic optoelectronics,[8,14–16] upcycling and reprocessing,[17,18] 3D printing,[19,20] templating 1D structures,[21] energy storage,[22,23] soft robotics,[24,25] wearable electronics,[26–28] pressure-sensitive adhesives,[29–31] and biomedical devices.[32–34] Theoretical and computational simulations offer valuable insights into the hierarchical structure and complex dynamics of these systems, complementing experimental observations and enabling a deeper understanding of their underlying mechanisms.[35–36]

Recently, we have explored the structural and mechanical properties of **ABA** linear-brush-linear triblock copolymers that form physical networks due to the microphase separation of bottlebrush middle blocks (**B**) and terminal linear blocks (**A**).[8,37] Despite their tissue-like softness and strain-stiffening, such networks possess a relatively low strength of $\sigma_{max} \cong 0.5$ MPa, which is an order of magnitude weaker than that of stress-supporting tissues such as skin and blood vessels. The low strength of **ABA** elastomers is due to the so-called "one strand – one molecule" network assembly, where each bottlebrush backbone forms only one mechanically active strand between the network nodes formed by aggregated **A** blocks. These shortcomings can be eliminated by switching to bottlebrush graft copolymers (**A**-g-**B**), where linear **A** blocks are randomly grafted along the backbone of the bottlebrush **B** block. These macromolecules self-assemble into a network, where one bottlebrush backbone spans multiple strands, yielding elastomers with up to 1 MPa strength.[19] However, despite the improved strength, the studied **A**-g-**B** copolymers exhibited moderate strain-stiffening (β<0.5), which corresponded to a lower bound of biological tissues. Therefore, it is

A. Z. Umarov, E. A. Nikitina, D. A. Ivanov
Faculty of Chemistry
Lomonosov Moscow State University (MSU)
GSP-1, 1–3 Leninskiye Gory, Moscow 119991, Russian Federation
E-mail: dimitri.ivanov@uha.fr
J. Collins, A. V. Dobrynin, S. S. Sheiko
Department of Chemistry
University of North Carolina at Chapel Hill
Chapel Hill, NC 27599-3290, USA
I. Moutsios, D. A. Ivanov
Institut de Sciences des Matériaux de Mulhouse-IS2M
CNRS UMR 7361, Mulhouse F-68057, France
M. Rosenthal
Department of Chemistry
KU Leuven
Celestijnenlaan 200F, Leuven Box 2404, B-3001, Belgium

The ORCID identification number(s) for the author(s) of this article can be found under https://doi.org/10.1002/marc.202400569

DOI: 10.1002/marc.202400569

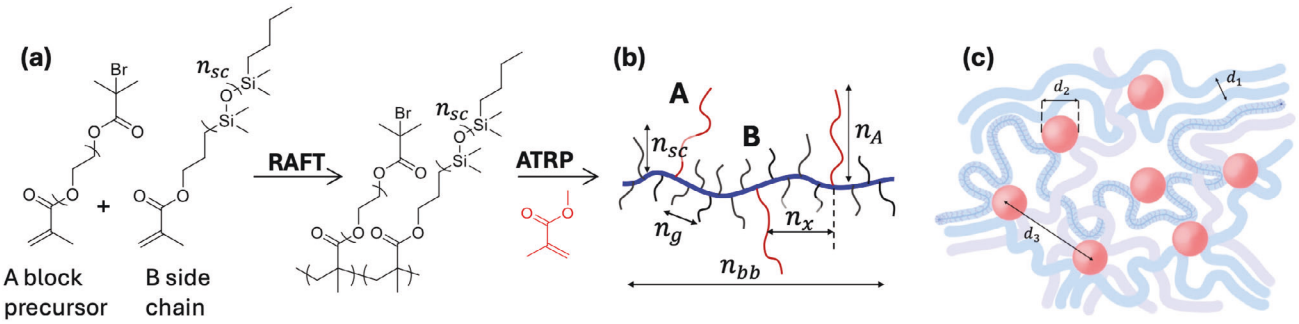

Figure 1. a) Controlled radical polymerization of assorted macromonomers yields c) **A**-g-**B** brush-like graft copolymers with controlled grafting density of the PDMS brush b) block and fraction of linear PMMA A blocks distributed as long side chains in the brush block. c) Microphase separation of the PMMA and PDMS block results in the formation of a physical network linked by PMMA domains dispersed in the PDMS bottlebrush matrix.

vital to find network (re)configuration pathways toward enhancement of the strain-stiffening behavior.

There are several methods that are commonly used to improve the packing of block copolymers (BCP), including thermal, vapor, and selective solvent annealing.[38–40] Thermal annealing is not very efficient due to an exponential decay of chain mobility with increasing segregation strength, resulting in kinetically trapped morphologies.[39,41] Annealing in solvent vapor significantly improves the microdomain order in thin BCP films,[42] however it does not work for bulk samples, requiring considerable time for swelling. Structural reorganization can be facilitated by direct immersion of BCP films in selective solvents.

Herein, we study the evolution of structure and mechanical properties for a series of bottlebrush graft-copolymers containing polydimethylsiloxane (PDMS) side chains polymethyl methacrylate (PMMA) linear blocks during thermal annealing and direct immersion in selective solvents. The objective of the work is to find an optimal strategy to achieve the structural reconfiguration of self-assembled networks, resulting in an enhanced strain-stiffening behavior to better mimic the mechanical properties of soft biological tissues. It is important to note that swelling in a selective solvent allows network reconfiguration without its disassembly, which is vital for practical applications relying on sample integrity.

2. Results and Discussion

2.1. Composition and Morphology of A-g-B Brush Networks

We synthesized a series of **A**-g-**B** graft copolymers using a combination of reversible addition-fragmentation chain transfer (RAFT) co-polymerization of polydimethylsiloxane (PDMS) and Br-terminated poly(ethylene glycol) (PEG) macromonomers, followed by atom transfer radical polymerization (ATRP) of poly(methyl methacrylate) (PMMA) A-block grafted from the terminal bromine (**Figure 1a**).[19] This yielded poly[MMA-g-(PDMS/PMMA)] bottlebrush graft copolymers (Figure 1b) with $n_g = 1$, volume fraction of the linear block ranging from 1.5 to 4.4%, and long backbone with a degree of polymerization (DP) varying from $n_{bb} = 210$ to 1935 (**Table 1**).

The **A**-g-**B** graft copolymers microphase-separate to form a physical network, where one macromolecule may span several network meshes (Figure 1c).[19] Copolymers with a low volume fraction of PMMA grafts form spherically shaped PMMA nanodomains that are covalently attached to the bottlebrush backbones. This configuration leads to increased crowding of the bottlebrush blocks at the interface of the PMMA domains, resulting in a much smaller interfacial surface area per bottlebrush segment compared to similar **ABA** systems.[19]

Table 1. Structural parameters of the studied bottlebrush graft-copolymers.

Sample	n_A [a]	φ_A [b]	n_g [c]	n_x [d]	n_{bb} [e]
Variation of n_A at constant n_x and n_{bb}					
A1	27	0.015	1	149	1935
A2	62	0.034	1	149	1935
A3	81	0.044	1	149	1935
Variation of n_{bb} at constant n_x and similar n_A					
B1	53	0.029	1	149	210
B2	63	0.034	1	149	607
A2	62	0.034	1	149	1935

[a] Number average degree of polymerization (DP) of PMMA side chains as determined by ^{1}H-NMR; [b] Volume fraction of PMMA, $\rho_{PMMA} = 1.15$ g mL^{-1}, $\rho_{PDMS} = 0.96$ g mL^{-1}; [c] Number of spacer repeat units between A blocks; [d] Number average DP of brush backbone between PMMA side chains; and [e] DP of total brush backbone in the A-g-B macromolecule.

2.2. Network Reconfiguration upon Direct Immersion in a Selective Solvent

In this section, we describe the evolution of the structure and mechanical properties of the PMMA-g-PDMS elastomers upon swelling in different solvents selective to **A** and **B** blocks. Initially, the samples were cast from toluene, a non-selective solvent to both blocks and subjected to thermal annealing.

2.2.1. Thermal Annealing

The results of an in-situ heating-cooling experiment, exemplified for sample A1, are illustrated in **Figure 2**. The SAXS curves show

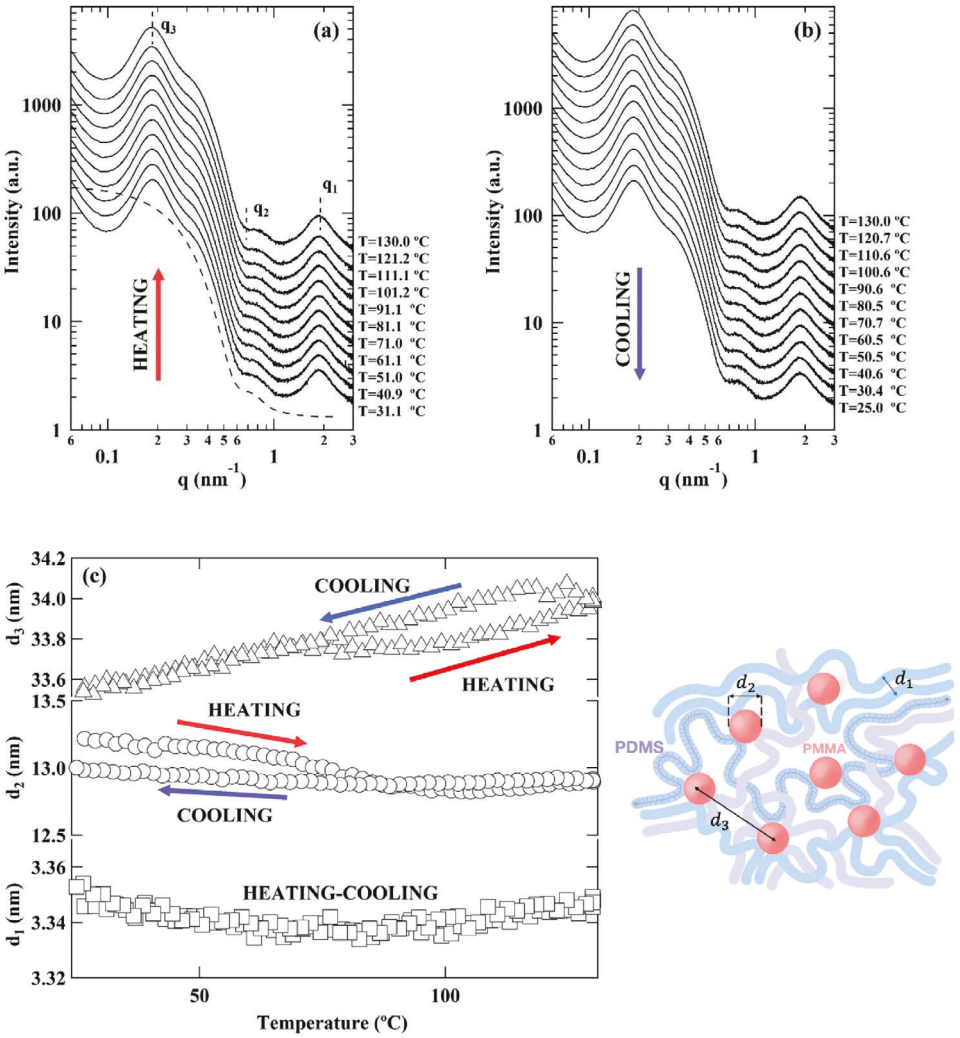

Figure 2. SAXS profiles corresponding to a) heating and b) cooling of sample A1 (n_A = 27, n_x = 149, n_{bb} = 1935). Dashed line in a) represents the fit of the curve at RT with the form-factor of polydisperse spheres. (c) Temperature dependencies of distances d_3, d_2 and d_1. A schematic of the network structure with indications of distances d_1, d_2, and d_3 is provided on the right.

the following features: a primary interference peak at q_3, corresponding to a d-spacing (d_3); the form factor of PMMA spheres with a diameter (d_2), with the first minimum at q_2; and a bottlebrush peak at q_1, corresponding to a d-spacing (d_1). These features are illustrated in the figure. These structural features align with previous observations reported in refs.[8, 43] The diameter of the PMMA domains was determined from the curves by fitting them to the form factor of spheres.

$$P(q) = 3\left[sin(qR) - qRcos(qR)\right]/(qR)^3 \quad (1)$$

The analytical expression in Equation (1) was convoluted with a Gaussian distribution to account for the scattering from a polydisperse population of spheres. A typical form factor resulting from the fit is depicted in Figure 2A with a dashed line, suggesting PMMA spheres ≈13 nm in diameter, separated by a distance of ≈33 nm. Within the bottlebrush matrix, the backbones are separated by a characteristic distance of d_1 = 3.3 nm. The sample was subjected to thermal cycling between room temperature and 130 °C, during which in-situ SAXS curves were continuously recorded (Figure 2). It is evident that thermal annealing does not significantly alter the SAXS curve (cf. Figure 2a,b). The observed variations of the characteristic distances d_3, d_2, and d_1 do not exceed 1.5% (Figure 2c). This demonstrates that the structure of the graft copolymer remains largely unaffected by thermal annealing even above the glass transition of the PMMA block, which is consistent with the lack of significant changes in mechanical properties upon annealing up to 170°C (Figure S3, Supporting Information). An additional variable-temperature SAXS experiment performed up to 200°C demonstrates that the structure of sample A1 remains stable, showing no significant changes as a result of the annealing process (Figure S5, Supporting Information).

2.2.2. Selective Solvent Annealing

Hexane and acetone were chosen as solvents to selectively swell the PDMS matrix and PMMA domains, respectively

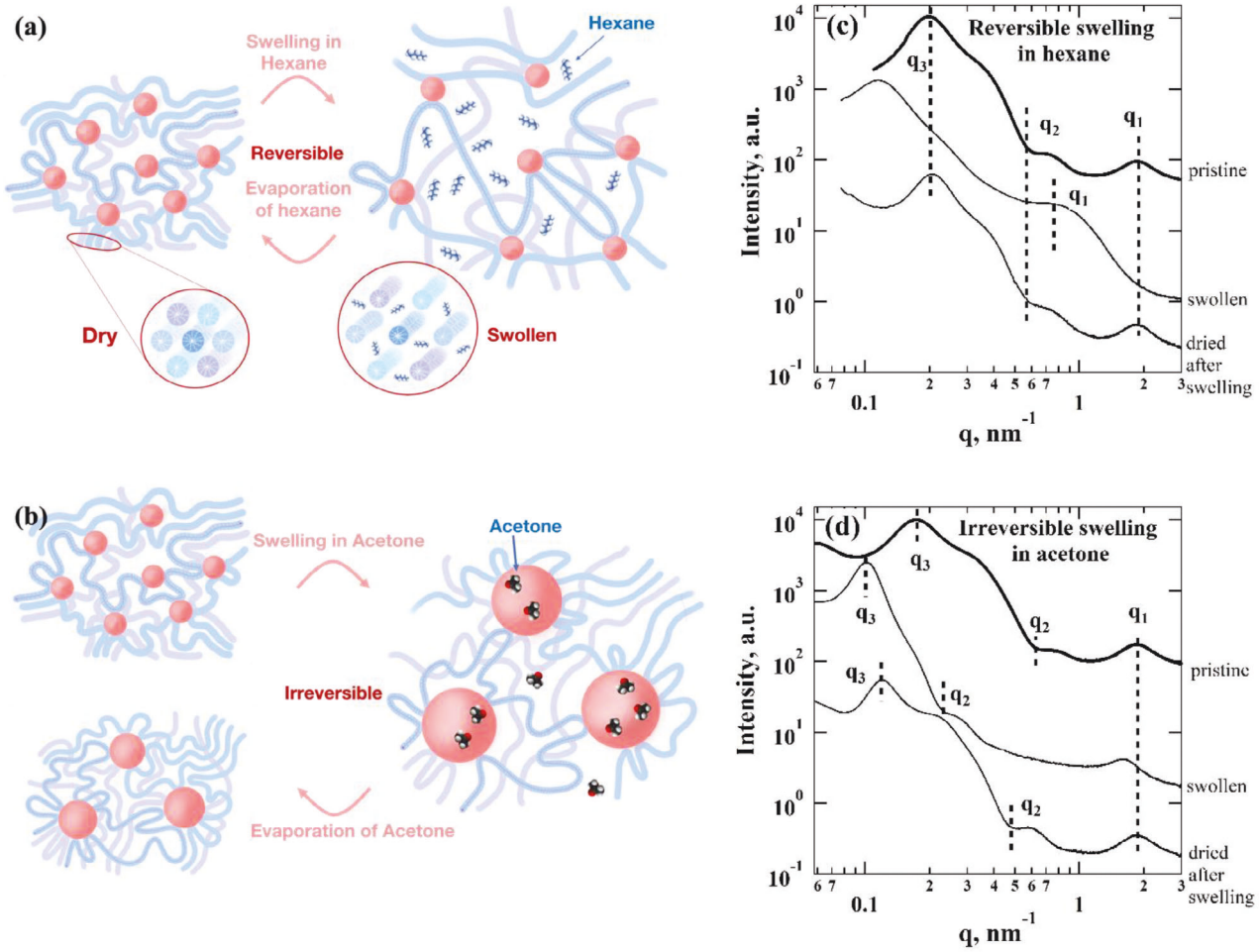

Figure 3. Annealing **A**-g-**B** elastomers in selective solvents. a) Annealing in hexane (selective to PDMS side chains) results in reversible swelling of the bottlebrush matrix. b) Annealing in acetone (selective to the PMMA linear **A** block) results in irreversible re-assembly of the **A** domains. The corresponding SAXS profiles are exemplified for samples B2 c) and A1 d) in their as-prepared condition, as well as in their swollen state in hexane and acetone. The SAXS curves corresponding to post-dried samples are also included to evaluate the reversibility of the swelling process. The structural parameters d_1, d_2, and d_3 are depicted in Figure 1b.

(**Figure** 3a,b). Theresults of in-situ X-ray scattering experiments during swelling and subsequent drying of the samples are presented in Figure 3c,d. Taking sample B2 as an example (Figure 3c), it can be seen that swelling in hexane significantly increases the distances d_3 and d_1, while the size of the PMMA spheres remains practically unaffected. The latter conclusion is deduced from the fact that the first minimum of the form-factor of spheres does not shift (dashed line d_2 in Figure 3a). Such behavior is expected, as hexane should only swell the PDMS matrix of the graft-copolymer. Moreover, the swelling-caused morphological changes are fully reversible (Figure 3a) as evidenced by the nearly complete similarity between the pristine and dried X-ray curves (Figure 3c).

In contrast, swelling in acetone caused substantial network rearrangement, which was irreversible after evaporation (Figure 3b). Since acetone selectively swells only the PMMA domains, both d_3 and d_2 are increased as exemplified by sample A1 (Figure 3d). Furthermore, the final structure formed after drying from acetone is visibly different from the initial one, characterized by significantly increased d_3 and d_2. Specifically, upon a swelling-evaporation cycle of sample A3 in acetone, the d_2 spacing increases from 13.5 to 17.2 nm, while d_3 increases from 26.3 to 39.6 nm. This increase in the d_3-distance is corroborated by the corresponding low-q shift of the main maximum of the SAXS structure factor (Figure S4, Supporting Information). One can view the swelling of **A** domains as a process toward an inverse micellar structure,[44] where PMMA grafts play the role of corona blocks stabilizing the cores of interconnected PDMS domains. This structural reorganization results in an increase in the domain size as well as the distance between them due to the stretching of the PDMS bottlebrush strands to satisfy the packing constraints.

The stretching of the PDMS blocks in the PMMA-selective solvent (acetone) is corroborated by a significant enhancement of the strain-stiffening behavior (**Figure** 4). The stress-elongation curves were analyzed by using the equation of state,[8] describing

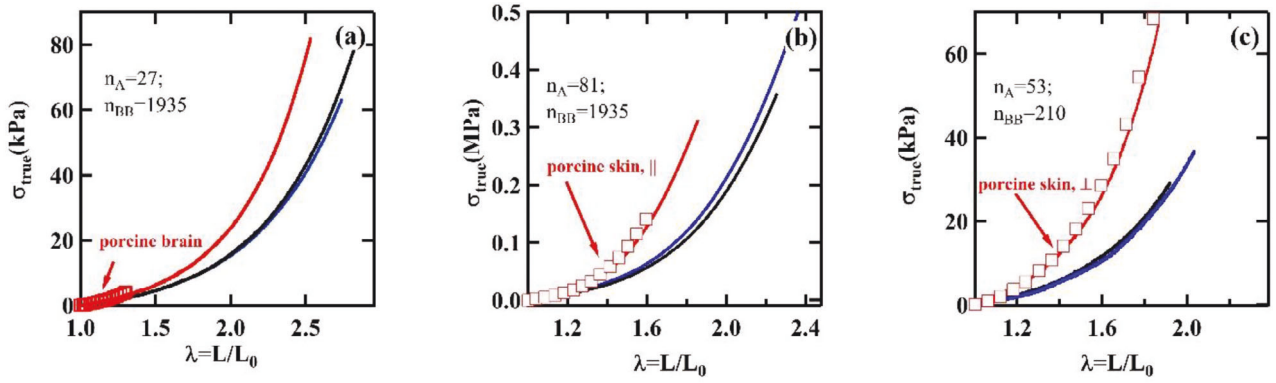

Figure 4. Impact of solvent annealing on mechanical properties of the bottlebrush graft-copolymer. Black curves represent the initial sample, blues curves- the samples after immersion in hexane for 30 min and subsequent drying, and red curves- the samples after immersion in acetone for 30 min and subsequent drying. The acetone-annealed sample A1 in a) replicates the mechanics of the porcine brain,[46] while samples A3 and B1 in b,c) display a perfect match with the porcine skin measured perpendicular and parallel to the spine line, respectively.[47]

the evolution of the true stress with the elongation ratio λ at a constant volume as

$$\sigma_{true}\ (\lambda) = \frac{G}{3}\ \left(\lambda^2 - \lambda^{-1}\right)\left(1 + 2\left(1 - \frac{\beta\left(\lambda^2 + 2\lambda^{-1}\right)}{3}\right)^{-2}\right) \quad (2)$$

In this expression, the structural shear modulus (G) and the strain-stiffening parameter β describe materials mechanical properties and are obtained from the fitting of the deformation curves. The strain-stiffening parameter $\beta = \langle R_{in}^2 \rangle / R_{max}^2$ is defined as a ratio of the mean square end-to-end distance, $\langle R_{in}^2 \rangle$, of undeformed strands to the square of their end-to-end distance in the fully stretched state, R_{max}.[45] The Young's modulus, E_0, at small deformations, $\lambda \to 1$, corresponding to Equation (2), is given by

$$E_0 = \ G\left(1 + 2(1-\beta)^{-2}\right) \quad (3)$$

For a small value of $\beta \ll 1$, it recovers the classical relationship between the Young's and shear modulus, $E_0 = \ 3G$, for incompressible systems.

Table 2. Variation of mechanical and structural parameters of the studied samples upon immersion annealing in hexane and acetone.

Treatment[a)]	E_0 (kPa)[b)]	B[c)]	λ_{max}[d)]	σ_{max} [kPa][e)]	d_1 [nm][f)]	d_2 [nm][g)]	d_3 [nm][h)]
Sample A1: n_A = 27, n_x = 149, n_{bb} = 1935							
pristine	7.7	0.33	2.86	84.4	3.35	13.3	36.1
hexane	7.2	0.33	2.74	66.5	3.35	13.3	36.1
acetone	9.3	**0.46**	2.53	82	3.35	17.8	52.4
Sample A2: n_A = 62, n_x = 149, n_{bb} = 1935							
pristine	31.4	0.40	2.92	605	32.2	15.2	3.4
hexane	28.8	0.41	2.96	542	31.8	14.8	3.4
acetone	34.8	**0.63**	2.09	256	46.2	20.0	3.4
Sample A3: n_A = 81, n_x = 149, n_{bb} = 1935							
pristine	45.3	0.53	2.26	359	3.35	13.6	27.6
hexane	56.8	0.50	2.48	627	3.35	13.45	26.2
acetone	62.4	**0.71**	1.86	313	3.35	17.8	52.4
Sample B1: n_A = 27, n_x = 149, n_{bb} = 1935							
pristine	12.8	0.42	1.92	29.2	3.35	13.2	28.6
hexane	10.8	0.45	2.04	38.4	3.35	13.3	28.6
acetone	22.9	**0.57**	1.87	67.0	3.35	16.0	38.1
Sample B2: n_A = 63, n_x = 149, n_{bb} = 607							
pristine	20.9	0.48	2.14	96.9	3.35	14.4	31.1
hexane	23.8	0.47	2.10	106	3.35	14.2	31.4
acetone	33.3	**0.62**	1.79	101	3.35	18.2	42

[a)] Non-treated (pristine) samples and samples annealed by direct immersion for 30 min in hexane or acetone and subsequently dried; [b)] Young's modulus determined either as the tangent of a stress–strain curve at $\lambda \to 1$ or from the fitting Equation (3) at λ = 1; [c)] Strain-stiffening parameter obtained by fitting stress–strain curves with Equation (2); [d)] Elongation at break; [e)] Stress at the break; and [f–h)] Microstructural parameters d_1, d_2 and d_3 (Figure 1B), extracted from SAXS measurements.

The fitting results are summarized in **Table 2**. The annealing in hexane does not cause significant changes in mechanical properties, which is consistent with the X-ray data. In contrast, selective swelling in acetone brings about a significant increase in β from 0.40 to 0.63, which is consistent with the d_3 increase from 32.2 to 46.2 nm. The bottlebrush strands connecting the A domains become more extended, i.e. larger $\langle R_{in}^2 \rangle$, resulting in a stronger strain-stiffening effect. The achieved level of strain-stiffening in acetone-annealed elastomers allowed for exact matching of the deformation response of soft tissues such as porcine skin and brain tissue (Figure 4).

2.3. Dimensionality of Swelling in a Matrix-Selective Solvent

To address the details of the swelling process in graft-copolymers, it is instructive to correlate the degree of swelling with the structure evolution. Such correlations were established by monitoring the swelling-drying process in hexane with in-situ synchrotron SAXS using a specially designed liquid cell. Considering d_3 as a characteristic mesh size of the network structure, one can write:

$$\frac{V_{sw}}{V_{dry}} \sim \frac{d_{3,sw}^3}{d_{3,\,dry}^3} \tag{4}$$

where $Q_{vol} = \frac{V_{sw}}{V_{dry}}$ is the ratio of the macroscopic volumes of the swollen and dry samples ($V_{sw} = V_{dry} + V_{solvent}$), and $d_{3,sw}$ and $d_{3,dry}$ are the corresponding distances d_3. Since the swelling in hexane involves only the bottlebrush matrix (V_{BB}), one can be written:

$$\frac{V_{BB,\,sw}}{V_{BB,dry}} \sim \frac{d_{3,sw}^3 - \varphi d_{3,\,dry}^3}{(1-\varphi)\, d_{3,\,dry}^3} \tag{5}$$

where the volume fraction φ occupied by the physical nodules is excluded from the swelling ratio. The swelling of the bottlebrush matrix can also be determined from the dilatation of d_1 which is proportional to the parameter of the 2D unit cell formed by neighboring bottlebrushes. In this model, it is implied that the contour length of the bottlebrush backbones does not change with swelling and that they pack as rigid cylinders on a 2D lattice. Therefore, the swelling ratio can be expressed as:

$$\frac{V_{BB,\,sw}}{V_{BB,dry}} \sim \frac{d_{1,sw}^2}{d_{1,\,dry}^2} \tag{6}$$

If the model is correct, one can expect that

$$\frac{d_{1,sw}^2}{d_{1,\,dry}^2} \sim \frac{d_{3,sw}^3 - \varphi d_{3,\,dry}^3}{(1-\varphi)\, d_{3,\,dry}^3} \tag{7}$$

One of the ways to validate the model and, consequently Equation (7), is to directly compare the swelling ratio of a graft-copolymer sample with the corresponding variation of d_1 and d_3.

The mass swelling ratio Q_{mass} is measured by directly weighing the dry and swollen samples as:

$$Q_{mass} = \frac{m_{sw}}{m_{dry}} \tag{8}$$

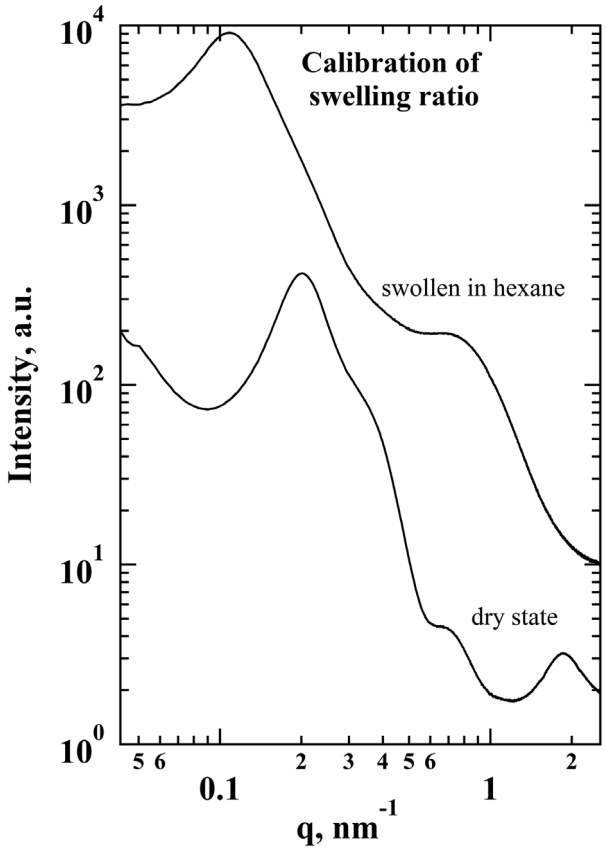

Figure 5. SAXS curves of sample A2 in the dry state, as well as swelling in hexane at volume swelling ratio $Q_{vol} = 5.96$.

where the mass ratio is related to the corresponding volumes by the following equation, including the mass densities of the solvent and polymer (ρ_{sol} and ρ_{pol})

$$\frac{M_{sw}}{M_{dry}} = \frac{V_{solvent}\rho_{sol} + V_{pol}\rho_{pol}}{V_{pol}\rho_{pol}} = [Q_{vol} - 1]\frac{\rho_{sol}}{\rho_{pol}} + 1 \tag{9}$$

Therefore, Q_{vol} can be expressed as:

$$Q_{vol} = \left[Q_{mass} - 1\right] \frac{\rho_{pol}}{\rho_{solvent}} + 1 \tag{10}$$

The results of such verification are exemplified for sample A2 in **Figure 5** and **Table 3**.

It is evident that the estimates of the volume swelling ratio from the sample weight and from the spacings d_3 and d_1 are in

Table 3. Correlation between the macroscopic and microscopic swelling ratios measured for sample A2.

Sample state	d_1[nm]	d_3[nm]	Q_{vol}[a)]	$\frac{d_{3,sw}^3 - \varphi d_{3,\,dry}^3}{(1-\varphi) d_{3,\,dry}^3}$	$\frac{d_{1,sw}^2}{d_{1,\,dry}^2}$
dry	3.4	32.0	5.96	5.94	6.38
swollen	8.5	57.4			

[a)] Swelling ratio Q_{vol} is calculated from Q_{mass} using Equation (10).

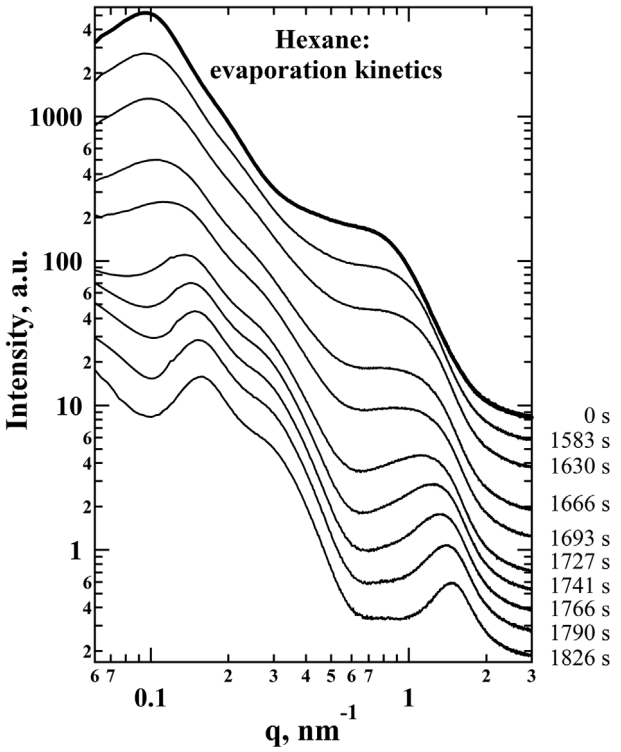

Figure 6. In situ SAXS experiment on the drying of sample A1, which was initially swollen in hexane.

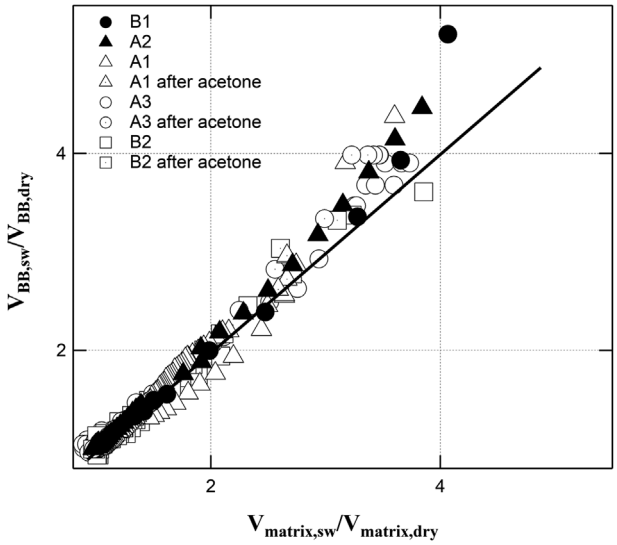

Figure 7. Concurrent 3D swelling of the bottlebrush nodular structure in hexane (see Equation 6) and two-dimensional swelling of the bottlebrush matrix (see Equation 8) are observed. The notation 'after acetone' indicates that the samples were immersion-annealed in acetone prior to swelling in hexane.

good agreement with each other, which supports the model and eliminates the need to weigh the sample at each stage of swelling.

Figure 6 shows the results of a typical SAXS experiment during which sample A1, initially swollen in hexane, was drying. The curves indicate gradually decreasing distances d_3 and d_1 in the course of the drying process (cf. frames 0 through 90).

The results of all in-situ drying experiments are displayed in **Figure 7**. It can be seen that most of the data merge on the line y = x in the coordinates of the $V_{BB,\,sw}$ versus $V_{matrix,\,sw}$ normalized by the corresponding values in the dry state. This shows that the model of concurrent 3D swelling of the nodular structure and 2D swelling of the spacing between bottlebrush backbones is valid.

If one analyzes Figure 7 more closely, a deviation from linearity can be noticed for sample B1, which contains the shortest bottlebrush block. We speculate that in this case, the bottlebrush block is in the most extended conformation. The observed deviation can be explained by the further stretching of the bottlebrush backbones, which starts to become significant at a certain stage of swelling. The deviation can be rationalized using the following equation:

$$\frac{V_{matrix,\,sw}}{V_{matrtix,dry}} \sim \frac{d^2_{1,sw}}{d^2_{1,\,dry}} \frac{\sqrt{\beta_{sw}}}{\sqrt{\beta_{dry}}} \tag{11}$$

Equation (11) takes into account not only the 2D swelling of the distance between bottlebrush backbones but also the possible stretching of the bottlebrush backbone. It is then instructive to plot the ratio $\frac{V_{matrix,\,sw}}{V_{matrtix,dry}} \frac{d^2_{1,dry}}{d^2_{1,\,sw}}$ as a function of the swelling ratio in order to monitor the variation of β (see **Figure 8**).

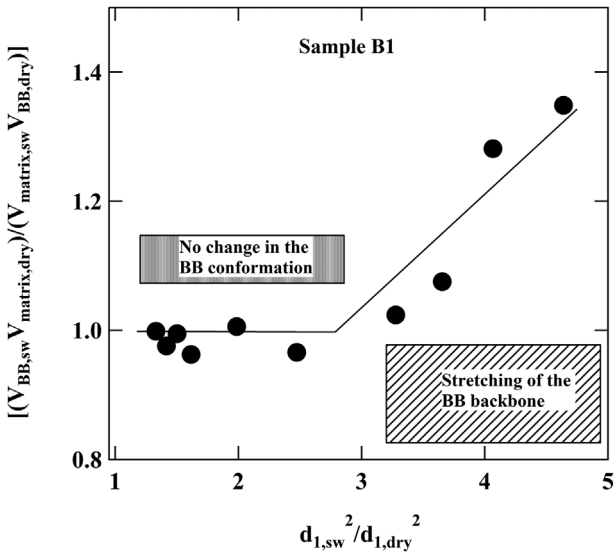

Figure 8. The ratio of the normalized volumes of the bottlebrush nodular structure and bottlebrush matrix as a function of the 2D swelling of the bottlebrush matrix. The deviation from unity indicates a change in the conformation of the bottlebrush backbone.

Figure 8 shows that the experimental data starts to deviate from unity for the matrix swelling ratios above approximately three. This upward turn corresponds to a noticeable increase in the stiffening parameter (β) and indicates a significant change in the conformation of the bottlebrush backbone occurring during swelling. It can be seen that $\sqrt{\beta_{sw}}/\sqrt{\beta_{dry}}$ reaches ca. 1.34 at the highest extent of swelling, which is equivalent to the increase of β_{sw} by ca. 1.8 times. Using the value of β obtained by fitting the stress–strain curves with Equation (2) (cf. Table 2) it can be

concluded that at the highest extent of swelling the value of β reaches approximately 0.76.

3. Conclusion

In this work, we study the effect of annealing on the mechanical and structural properties of bottlebrush graft copolymers. It was shown that the strain-stiffening parameter (β) can be significantly increased up to 0.7 by treating the materials in a solvent selective for the linear **A** blocks grafted to the brush **B** block. This allows for bringing the mechanical properties of the copolymers closer to those of soft biological tissues, such as the brain and skin. The structural reorganization of the self-assembled networks was monitored by the real-time synchrotron small-angle X-ray scattering. This showed that selective solvent annealing resulted in a substantial, irreversible reconfiguration of the spherical domains of grafted side chains in the bottlebrush matrix, leading to an increase in domain size and the distance between them. In contrast, the evolution of the structure in a selective solvent for the bottlebrush matrix was found to be reversible. The data for all studied samples merged onto a single straight line, indicating that the bottlebrush nodular structure was undergoing 3D swelling, whereas the bottlebrush matrix displayed a 2D swelling characteristic of the spacing increase between bottlebrush backbones.

4. Experimental Section

Synthesis: Two series of samples with systematically varied degrees of polymerization of brush backbone (n_{bb}) and linear **A** block (n_A) were made by first synthesizing a bromine-terminated PEG macromonomer to be used as an ATRP initiating site for growing the PMMA blocks. Using a two-step polymerization where first grafting through RAFT of the PDMS macromonomer and the bromine terminated PEG macromonomer were copolymerized to each of the targeted n_{bb}'s. Next, the brush polymers were used as macroinitiators with the bromine-terminated PEG sidechains serving as initiating sites for grafting from ATRP of linear MMA. A full detailed description of the synthesis can be found in the previous publication.[19]

Small-Angle X-ray Scattering (SAXS): The SAXS experiments were carried out at the BM26 beamline of the European Synchrotron Radiation Facility (ESRF) in Grenoble (France). The measurements were conducted in transmission geometry using a photon energy of 12 keV. The accessed q values, with $|q| = 4\pi \sin(\theta)/\lambda$, where θ is the Bragg angle and λ is the wavelength, cover a range from 8.0×10^{-2} nm^{-1} to 4.0 nm^{-1}. A Pilatus 1M detector (169 mm x 179 mm active area) was employed for recording SAXS intensity at a sample-to-detector distance of 3 m. The swelling/drying experiments in selective solvents were performed with a custom-built liquid cell.

Solvent Annealing: The **A**-g-**B** elastomers were dissolved in toluene and poured into Teflon petri dishes and left to dry for 3 days under ambient conditions. The samples were removed from the dishes and a dog bone-shaped cutter (bridge dimensions: 12 mm x 2 mm x 1 mm) was used to punch out samples. The dog-bone-shaped samples were then individually placed on Teflon sheets and put in glass petri dishes filled with either acetone or hexane and left immersed in the solvent for 30 min. After this time, samples were removed from the solvent dishes and left to dry under ambient conditions and periodically weighed until a constant mass was reached.

Mechanical Tests: Dog bone-shaped samples with bridge dimensions of 12 mm × 2 mm × 1 mm were loaded into an RSA-G2 DMA (TA Instruments) and subjected to uniaxial extension at 20 °C and a constant strain rate of 0.005 s^{-1}. Samples were stretched until rupture, delivering the entire mechanical profile. In each case, tests were conducted in triplicate to ensure the accuracy of the data. All stress–elongation curves show the dependence of the true stress σ_{true} on the elongation ratio λ in accordance with Equation (2) at small and intermediate deformation ranges, but switch to a linear scaling with λ at the later stages of deformation. The elongation ratio λ for uniaxial network deformation is defined as the ratio of the sample's instantaneous size L to its initial size L_0, $\lambda = L/L_0$.

Supporting Information

Supporting Information is available from the Wiley Online Library or from the author.

Acknowledgements

The authors acknowledge the European Synchrotron Radiation Facility (ESRF) for the provision of synchrotron radiation facilities and would like to thank the personnel of the BM26 beamline for the excellent technical support. A.Z.U., E.A.N., and D.A.I. acknowledge the Russian Science Foundation (RSF grant 23-73-30005). S.S. and A.V.D. acknowledge funding from the National Science Foundation (DMR 2004048 and DMR 2324167).

Conflict of Interest

The authors declare no conflict of interest.

Data Availability Statement

The data that support the findings of this study are available from the corresponding author upon reasonable request.

Keywords

bottlebrush correlation peak, bottlebrush graft-copolymers, selective solvent, small-angle X-ray scattering, swelling

Received: July 12, 2024
Revised: September 14, 2024
Published online: October 10, 2024

[1] L. G. Griffith, G. Naughton, *Science* **2002**, *295*, 1009.
[2] S. Lv, D. M. Dudek, Y. Cao, M. M. Balamurali, J. Gosline, H. Li, *Nature* **2010**, *465*, 69.
[3] R. Verduzco, X. Li, S. L. Pesek, G. E. Stein, *Chem. Soc. Rev.* **2015**, *44*, 2405.
[4] S. Tu, C. K. Choudhury, I. Luzinov, O. Kuksenok, *Curr. Opin. Solid State Mater. Sci* **2019**, *23*, 50.
[5] I. Lapkriengkri, K. R. Albanese, A. Rhode, A. Cunniff, A. A. Pitenis, M. L. Chabinyc, C. M. Bates, *Annu. Rev. Mater. Res.* **2024**, *54*, 27.
[6] M. G. Karavolias, M. K. Mahanthappa, *Phys. Rev. Mater.* **2024**, *8*, 015603.
[7] H. Joodaki, M. B. Panzer, *Proc. Inst. Mech. Eng. Part H.* **2018**, *232*, 323.
[8] M. Vatankhah-Varnosfaderani, A. N. Keith, Y. Cong, H. Liang, M. Rosenthal, M. Sztucki, C. Clair, S. Magonov, D. A. Ivanov, A. V. Dobrynin, S. S. Sheiko, *Science* **2018**, *359*, 1509.
[9] W. F. M. Daniel, J. Burdyńska, M. V. Vatankhah-Varnoosfaderani, K. Matyjaszewski, J. Paturej, M. Rubinstein, A. V. Dobrynin, S. S. Sheiko, *Nat. Mater.* **2016**, *15*, 183.

[10] M. Abbasi, L. Faust, M. Wilhelm, *Adv. Mater.* **2019**, *31*, 1806484.
[11] S. S. Sheiko, A. V. Dobrynin, *Macromolecules* **2019**, *52*, 7531.
[12] S. S. Sheiko, A. Keith, C. Clair, A. Lallam, E. Bersenev, D. Ivanov, Y. Tian, A. Dobrynin, *Macromolecules* **2020**, *53*, 9306.
[13] T. Pakula, Y. Zhang, K. Matyjaszewski, H.-i. Lee, H. Boerner, S. Qin, G. C. Berry, *Polymer* **2006**, *47*, 7198.
[14] E. R. Sauvé, C. M. Tonge, Z. M. Hudson, *J. Am. Chem. Soc.* **2019**, *141*, 16422.
[15] A. L. Liberman-Martin, C. K. Chu, R. H. Grubbs, *Macromol. Rapid Commun.* **2017**, *38*, 1700058.
[16] B. B. Patel, D. J. Walsh, D. H. Kim, J. Kwok, B. Lee, D. Guironnet, Y. Diao, *Sci. Adv.* **2020**, *6*, eaaz7202.
[17] C. Choi, J. L. Self, Y. Okayama, A. E. Levi, M. Gerst, J. C. Speros, C. J. Hawker, J. Read de Alaniz, C. M. Bates, *J. Am. Chem. Soc.* **2021**, *143*, 9866.
[18] D. Zhang, F. Vashahi, E. Dashtimoghadam, X. Hu, C. Wang, J. Garcia, A. V. Bystrova, M. Vatankhah-Varnoosfaderani, F. A. Leibfarth, S. S. Sheiko, *Angew. Chem., Int. Ed.* **2022**, e202217941.
[19] E. Dashtimoghadam, M. Maw, A. N. Keith, F. Vashahi, V. Kempkes, Y. D. Gordievskaya, E.Yu. Kramarenko, E. A. Bersenev, E. A. Nikitina, D. A. Ivanov, Y. Tian, A. V. Dobrynin, M. Vatankhah-Varnosfaderani, S. S. Sheiko, *Mater. Horiz.* **2022**, *9*, 3022.
[20] C. Choi, Y. Okayama, P. T. Morris, L. L. Robinson, M. Gerst, J. C. Speros, C. J. Hawker, J. Read de Alaniz, C. M. Bates, *Adv. Funct. Mater.* **2022**, *32*, 2200883.
[21] M. Müllner, A. H. Müller, *Polymer* **2016**, *98*, 389.
[22] S. Li, K. Jiang, J. Wang, C. Zuo, Y. H. Jo, D. He, X. Xie, Z. Xue, *Macromolecules* **2019**, *52*, 7234.
[23] X. Lin, G. Xie, S. Liu, M. R. Martinez, Z. Wang, H. Lou, R. Fu, D. Wu, K. Matyjaszewski, *ACS Appl. Mater. Interfaces* **2019**, *11*, 18763.
[24] G. M. Whitesides, *Angew. Chem., Int. Ed.* **2018**, *57*, 4258.
[25] M. Vatankhah-Varnosfaderani, W. F. M. Daniel, A. P. Zhushma, Q. Li, B. J. Morgan, K. Matyjaszewski, D. P. Armstrong, R. J. Spontak, A. V. Dobrynin, S. S. Sheiko, *Adv. Mater.* **2017**, *29*, 1604209.
[26] K. Xu, Y. Lu, K. Takei, *Adv. Mater. Technol.* **2019**, *4*, 1800628.
[27] M. L. Le, I. Lapkriengkri, K. R. Albanese, P. H. Nguyen, C. Tran, J. R. Blankenship, R.A Segalman, C. M. Bates, M.L Chabinyc, *Chem. Mater.* **2023**, *35*, 7301.
[28] P. Xu, S. Wang, A. Lin, H.-K. Min, Z. Zhou, D. Wenkun, S. Yu, H. Xi, H. Tran, X. Liu, *Nat. Comm.* **2023**, *14*, 623.
[29] M. Maw, A. Tanas, E. Dashtimoghadam, E. Nikitina, D. Ivanov, A. Dobrynin, M. Vatankhah-Varnosfaderani, S. Sheiko, *ACS Appl. Mater. Interfaces* **2023**, *15*, 41870.
[30] K. J. Arrington, S. C. Radzinski, K. J. Drummey, T. E. Long, J. B. Matson, *ACS Appl. Mater. Interf.* **2018**, *10*, 26662.
[31] H. Kim, J. J. Watkins, A. J. Crosby, *Soft Matter* **2023**, *19*, 5311.
[32] J.-W. Jeong, G. Shin, S. I. Park, K. J. Yu, L. Xu, J. A. Rogers, *Neuron* **2015**, *86*, 175.
[33] K. Scholten, E. Meng, *Lab Chip* **2015**, *15*, 4256.
[34] A. J. T. Teo, A. Mishra, I. Park, Y.-J. Kim, W.-T. Park, Y.-J. Yoon, *ACS Biomater. Sci. Eng.* **2016**, *2*, 454.
[35] I. V. Mikhailov, F. A. M. Leermakers, A. A. Darinskii, E. B. Zhulina, O. V. Borisov, *Macromolecules* **2021**, *54*, 4747.
[36] H. Kang, T. Pan, C. E. Sing, *Macromolecules* **2024**, *57*, 8240.
[37] A. N. Keith, M. Vatankhah-Varnosfaderani, C. Clair, F. Fahimipour, E. Dashtimoghadam, A. Lallam, M. Sztucki, D. A. Ivanov, H. Liang, A. V. Dobrynin, S. S. Sheiko, *ACS Cent. Sci.* **2020**, *6*, 413.
[38] R. J. Albalak, E. L. Thomas, M. S. Capel, *Polymer* **1997**, *38*, 3819.
[39] J. W. Jeong, W. I. Park, M.-J. Kim, C. A. Ross, Y. S. Jung, *Nano Lett.*. **2011**, *11*, 4095.
[40] W. I. Park, J. M. Kim, J. W. Jeong, Y. S. Jung, *ACS Nano* **2014**, *8*, 10009.
[41] T. P. Lodge, M. C. Dalvi, *Phys. Rev. Lett.* **1995**, *75*, 657.
[42] C. Sinturel, M. Vayer, M. Morris, M. A. Hillmyer, *Macromolecules* **2013**, *46*, 5399.
[43] C. Clair, A. Lallam, M. Rosenthal, M. Sztucki, M. Vatankhah-Varnosfaderani, A. N. Keith, Y. Cong, H. Liang, A. V. Dobrynin, S. S. Sheiko, D. A. Ivanov, *ACS Macro Lett.*. **2019**, *8*, 530.
[44] J. N. Israelachvili, *Intermolecular and Surface Forces*, 3rd Edition, **2011**, ISBN: 9780123919274.
[45] M. Maw, B. J. Morgan, E. Dashtimoghadam, Y. Tian, E. A. Bersenev, A. V. Maryasevskaya, D. A. Ivanov, K. Matyjaszewski, A. V. Dobrynin, S. S. Sheiko, *Macromolecules* **2022**, *55*, 2940.
[46] B. Rashid, M. Destrade, M. D. Gilchrist, *J. Mech. Behav. Biomed. Mater.* **2014**, *33*, 43.
[47] J. Lim, J. Hong, W. W. Chen, T. Weerasooriya, *Int. J. Impact. Eng.* **2011**, *38*, 130.